Cell

The *Drosophila* HP1 Homolog Rhino Is Required for Transposon Silencing and piRNA Production by Dual-Strand Clusters

Carla Klattenhoff,[1] Hualin Xi,[3,7,8] Chengjian Li,[2] Soohyun Lee,[3,7] Jia Xu,[3,6] Jaspreet S. Khurana,[1] Fan Zhang,[1] Nadine Schultz,[1] Birgit S. Koppetsch,[1] Anetta Nowosielska,[1] Herve Seitz,[2,4,5] Phillip D. Zamore,[2,*] Zhiping Weng,[3,*] and William E. Theurkauf[1,*]

[1]Program in Molecular Medicine and Program in Cell Dynamics
[2]Department of Biochemistry and Molecular Pharmacology and Howard Hughes Medical Institute
[3]Program in Bioinformatics and Integrative Biology
University of Massachusetts Medical School, Worcester MA, 01605, USA
[4]Laboratoire de Biologie Moléculaire Eucaryote, Université de Toulouse, Université Paul Sabatier, F-31000 Toulouse, France
[5]Laboratoire de Biologie Moléculaire Eucaryote, Centre National de la Recherche Scientifique, F-31000 Toulouse, France
[6]Department of Biomedical Engineering
[7]Bioinformatics Program
Boston University, Boston, MA 02215, USA
[8]Computational Science Center of Emphasis, Pfizer Inc, 620 Memorial Drive, Cambridge, MA 02139, USA
*Correspondence: phillip.zamore@umassmed.edu (P.D.Z.), zhiping.weng@umassmed.edu (Z.W.), william.theurkauf@umassmed.edu (W.E.T.)
DOI 10.1016/j.cell.2009.07.014

SUMMARY

Piwi-interacting RNAs (piRNAs) silence transposons and maintain genome integrity during germline development. In *Drosophila*, transposon-rich heterochromatic clusters encode piRNAs either on both genomic strands (dual-strand clusters) or predominantly one genomic strand (uni-strand clusters). Primary piRNAs derived from these clusters are proposed to drive a ping-pong amplification cycle catalyzed by proteins that localize to the perinuclear nuage. We show that the HP1 homolog Rhino is required for nuage organization, transposon silencing, and ping-pong amplification of piRNAs. *rhi* mutations virtually eliminate piRNAs from the dual-strand clusters and block production of putative precursor RNAs from both strands of the major 42AB dual-strand cluster, but not of transcripts or piRNAs from the uni-strand clusters. Furthermore, Rhino protein associates with the 42AB dual-strand cluster,but does not bind to uni-strand cluster 2 or *flamenco*. Rhino thus appears to promote transcription of dual-strand clusters, leading to production of piRNAs that drive the ping-pong amplification cycle.

INTRODUCTION

Mutations in the *Drosophila* piwi-interacting RNA (piRNA) pathway disrupt transposon silencing, cause DNA break accumulation during female germline development, and lead to defects in posterior and dorsoventral axis specification (Brennecke et al., 2007; Chambeyron et al., 2008; Klattenhoff et al., 2007; Vagin et al., 2006). The axis specification defects associated with piRNA pathway mutations are dramatically suppressed by mutations in *mnk* and *mei-41*, which encode Chk2 and ATR kinase homologs that function in DNA damage signaling (Chen et al., 2007; Klattenhoff et al., 2007; Pane et al., 2007). The developmental defects linked to piRNA pathway mutations thus appear to be secondary to DNA damage, which may result from transposon mobilization. PIWI proteins bind piRNAs, and mutations in genes encoding mouse and Zebrafish *piwi* homologs lead to transposon overexpression and germline-specific apoptosis (Carmell et al., 2007; Houwing et al., 2007), which could be triggered by DNA damage. The piRNA pathway may therefore have a conserved function in transposon silencing and maintenance of germline genome integrity.

Drosophila piRNAs appear to be derived from transposon rich clusters, most of which are localized in pericentromeric and subtelomeric heterochromatin (Brennecke et al., 2007). The majority of clusters produce piRNAs from both genomic strands (dual-strand clusters). However, two major clusters on the X chromosome produce piRNAs predominantly from one genomic strand (uni-strand clusters) (Brennecke et al., 2007; Brennecke et al., 2008). One of these uni-strand clusters maps to *flamenco,* a locus required for transposon silencing in the somatic follicle cells (Brennecke et al., 2007; Mevel-Ninio et al., 2007; Pelisson et al., 2007; Pelisson et al., 1994; Prud'homme et al., 1995; Sarot et al., 2004). The *flamenco* cluster contains fragments of a number of transposons, including *Zam*, *idefix*, and *gypsy*, and *flamenco* mutations disrupt silencing of these transposons (Desset et al., 2008; Mevel-Ninio et al., 2007; Prud'homme et al., 1995). In addition, transgenes carrying fragments of transposons in this cluster show *flamenco*-dependent silencing (Sarot et al., 2004). These findings suggest that piRNAs encoded by *flamenco trans*-silence complementary transposons located outside this cluster (Brennecke et al., 2007).

The mechanism of *trans*-silencing by piRNA is not well understood. piRNA-PIWI protein complexes catalyze homology-dependent target cleavage, suggesting that target transposon mRNAs are cotranscriptionally or posttranscriptionally degraded (Gunawardane et al., 2007; Saito et al., 2006). However, several *Drosophila* piRNA pathway mutations have been reported to modify position effect variegation (PEV) (Brower-Toland et al., 2007; Pal-Bhadra et al., 2002; Pal-Bhadra et al., 2004), which is linked to spreading of transcriptionally silent heterochromatin from pericentric and telomeric regions (Girton and Johansen, 2008). Piwi protein also binds to heterochromatin in somatic cells, and interacts with Heterochromatin protein-1 (HP1) in yeast two-hybrid and immunoprecipitation assays (Brower-Toland et al., 2007). piRNA-Piwi protein complexes could therefore silence target transposons by directing assembly of heterochromatin-like domains. In fission yeast, which do not have piRNAs, small interfering RNAs (siRNAs) and Argonaute 1 (Ago1) appear to recognize nascent transcripts at the centromere, triggering both transcript destruction and HP1 recruitment and assembly of centromeric heterochromatin (Buhler et al., 2006; Verdel and Moazed, 2005). A similar combination of homology dependent cleavage and heterochromatin assembly could drive piRNA based silencing in the *Drosophila* germline.

The mechanism of piRNAs biogenesis also remains to be fully elucidated. Dicer endonucleases cleave double-stranded precursors to produce miRNAs and siRNAs (reviewed in Ghildiyal and Zamore, 2009), but piRNA production is Dicer independent (Houwing et al., 2007; Vagin et al., 2006). A subset of sense and antisense piRNAs overlap by 10 base pairs and show a strong bias toward an A at position 10 of the sense strand and a complementary U at the 5′ end of the antisense strand, suggesting that positions 1 and 10 base pair (Brennecke et al., 2007; Gunawardane et al., 2007). As Argonautes cleave their targets between positions 10 and 11 of the guide strand (Gunawardane et al., 2007; Saito et al., 2006), these finding suggest that piRNAs are produced by a "ping-pong" amplification cycle in which antisense strand piRNAs bound to Argonaute proteins cleave complementary RNAs to produce the 5′ end of sense piRNAs, which in turn direct a reciprocal reaction that generates the 5′ end of antisense strand piRNAs (Brennecke et al., 2007; Gunawardane et al., 2007). However, most piRNAs cannot be assigned to ping-pong pairs, some clusters produce piRNAs from only one strand (Brennecke et al., 2007), and the mechanism of 3′ end generation has not been determined. It is also unclear how ping-pong amplification is initiated, since the cycle depends on pre-existing primary piRNAs.

Here, we show that Rhino (Rhi), a member of the Heterochromatin Protein 1 (HP1) subfamily of chromo box proteins (Volpe et al., 2001), is required for transposon silencing, production of piRNAs by dual-strand heterochromatic clusters, and efficient ping-pong amplification. Significantly, Rhi protein associates with the 42AB dual-strand cluster and is required for production of longer RNAs from both strands of this cluster. Rhi thus appears to promote expression of trigger RNAs that are processed to from primary piRNAs that drive ping-pong amplification and transposon silencing. We also show that protein coding genes carrying transposons and transposon fragments within introns escape silencing, suggesting that piRNA silencing is imposed after RNA processing. Furthermore, *rhi* mutations disrupt nuage, a perinuclear structure that is enriched in piRNA pathway components. We therefore speculate that the nuage functions as a perinuclear surveillance machine that scans RNAs exiting the nucleus and destroys transcripts with piRNA complementarity.

RESULTS

Drosophila piRNA pathway mutations lead to germline DNA damage and disrupt axis specification through activation of Chk2 and ATR kinases, which function in DNA damage signaling (Chen et al., 2007; Cook et al., 2004; Pane et al., 2007). Mutations in the *rhi* locus lead to very similar patterning defects (Volpe et al., 2001). The *mei-41* and *mnk* genes encode ATR and Chk2, respectively (Brodsky et al., 2004; Hari et al., 1995). To determine whether the axis specification defects associated with *rhi* result from damage signaling, we generated double mutants with *mnk* and *mei-41* and quantified axis specification by scoring for assembly of dorsal appendages, which are egg shell structures that form in response to dorsal signaling during oocyte development (Table S1 available online). Only 17% (n = 700) of embryos from rhi^{KG}/rhi^{2} females had two wild-type appendages. However, 80% (n = 689) of embryos from $mnk;rhi^{KG}/rhi^{2}$ double-mutant females had two appendages (Table S1). In addition, 33% (n = 732) of embryos from $mei\text{-}41;rhi^{KG}/rhi^{2}$ double-mutant females had two appendages (Table S1). Consistent with these observations, *rhi* mutations disrupt dorsal localization of Gurken and posterior localization of Vasa in the oocyte, and localization of both proteins is restored in $mnk;\ rhi^{KG}/rhi^{2}$ double mutants (Figure 1).

Both ATM and ATR kinases have been reported to activate Chk2 (Wang et al., 2006). Mutations in the *Drosophila atm* gene are lethal, but caffeine inhibits ATM and to a lesser extent ATR (Sarkaria et al., 1999). Strikingly, 88% (n = 473) of embryos from *rhi* mutant mothers fed caffeine had wild-type dorsal appendages (Table S1). Similarly, only 2% (n = 277) of embryos from *armi* mutant females had two dorsal appendages, compared with 11% (n = 477) after caffeine treatment (Table S1). In addition, 56% (n = 575) of embryos from $mei^{41D3}/mei^{41D3};\ armi^{72.1}/armi^{1}$ females had wild-type appendages, but 83% (n = 226) of embryos from $mei^{41D3}/mei^{41D3};\ armi^{72.1}/armi^{1}$ double mutants fed with caffeine had two appendages (Table S1). Caffeine combined with *mei-41* mutations thus leads to levels of suppression that are similar to *mnk* single mutations, suggesting that ATM and ATR redundantly activate Chk2 in *armi* and *rhi* mutants.

The *mei-W68* locus encodes the *Drosophila* Spo11 homolog, which is required for meiotic double-strand break formation (McKim and Hayashi-Hagihara, 1998). However, *mei-W68* mutations fail to suppress the dorsal appendage defects associated with *rhi* (Table S1), indicating that DNA damage signaling in *rhi* mutants is not due to defects in meiotic break repair.

The phosphorylated form of the *Drosophila* histone H2AX (γ−H2Av) accumulates near DNA double-strand break sites (Gong et al., 2005; Modesti and Kanaar, 2001; Redon et al., 2002). In wild-type ovaries, γ-H2Av foci are generally restricted to region 2 of the germarium, where meiotic double-strand breaks are formed (Figures 1D–1F) (Jang et al., 2003). As the

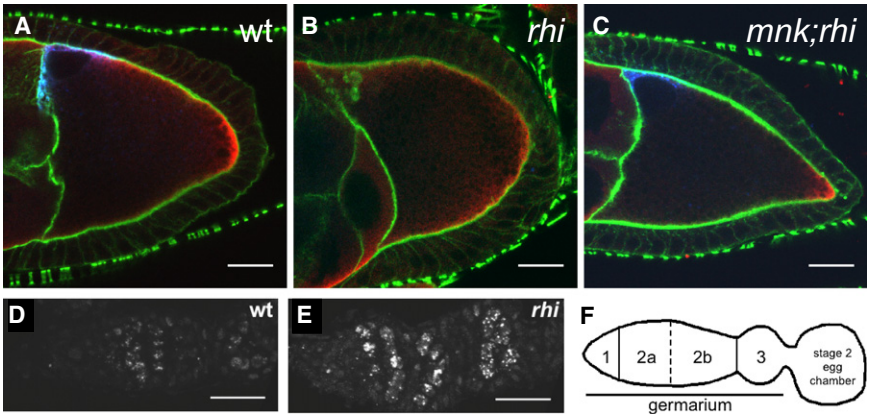

Figure 1. DNA Damage Signaling in *rhi* Mutants

(A–C) Mutations in *mnk*, which encodes the DNA damage signaling kinase Chk2, suppress the Gurken and Vasa protein localization defects in *rhi* mutants.

(A) In a stage 9 wild-type oocyte, Grk (blue) is localized at the dorsal anterior cortex near the oocyte nucleus and Vas (red) is localized at the posterior cortex. Actin filaments (green) mark the cell boundaries.

(B) In *rhi* egg chambers, this localization pattern is lost, with Grk and Vas dispersed throughout the oocyte.

(C) *mnk* suppresses the *rhi* phenotype, and rescues Grk and Vas localization during late oogenesis. Images were acquired under identical conditions. Projections of two serial 0.6 μm optical sections are shown. Scale bars represent 20 μm.

(D–F) *rhi* mutants have increased DNA damage in the germline.

(D) Foci of γ-H2Av are observed in wild-type ovaries in region 2a and 2b of the germarium and correspond to the DSBs induced during meiotic recombination.

(E) In *rhi* mutants, much larger foci also appear in region 2a of the germarium but persist in region 3 and the developing egg chambers. Samples were labeled and images were acquired under identical conditions. Projections of 5 serial 1μm optical sections are shown. Posterior is oriented to the right. Scale bars represent 10 μm.

(F) A schematic representation of the regions of the germarium and a developing egg chamber.

cysts mature and pass through region 3 of the germarium, γ-H2Av labeling is reduced. Stage 2 egg chambers, which bud from the germarium, show only low levels of γ-H2Av labeling. In *rhi* mutants, prominent γ-H2Av foci are present in germline cells of the germarium, and these foci persist and increase in intensity as cysts mature and bud to form stage 2 egg chambers (Figures 1D and 1E). *rhi* mutations thus appear to trigger germline-specific DNA breaks and damage signaling through ATM, ATR, and Chk2.

Transposon Silencing and Gene Expression

The piRNA pathway is required for transposon silencing in the *Drosophila* female germline (Vagin et al., 2006) but has also been implicated in heterochromatic gene silencing in somatic cells (Brower-Toland et al., 2007; Pal-Bhadra et al., 2002; Pal-Bhadra et al., 2004). We therefore assayed both transposon and protein-coding gene expression using whole-genome tiling arrays (Figure 2). In both *rhi* and armi mutants, most transposon families show a relatively modest 1.5- to 2-fold increase in expression, which is not statistically significant (false discovery rate [FDR] > 0.02). However, a subset of transposon families are dramatically overexpressed in both *rhi* and *armi* mutants (Figures 2B and 2C; blue points indicate FDR < 0.02). For example, *HeT-A* expression increased 70-fold in *rhino* and 117-fold in *armi* (Table S2). In total, 15 of 17 transposon families that are significantly overexpressed in *rhi* are also overexpressed in *armi* (Figure S1). 11 families are overexpressed with an FDR < 0.02 in *armi* mutants, but not in *rhi* (Figure S1). Rhino thus appears to silence a subset of the transposons silenced by Armi. This could reflect a role for Armi in transposon silencing in both somatic follicle cells and the germline (Klattenhoff et al., 2007), while Rhi appears to be restricted to the germline (see below).

Both *rhi* and *armi* mutations increased expression of long terminal repeat (LTR) elements, non-LTR retrotransposons, and inverted repeat (IR) elements (Figure S2) (Vagin et al., 2006), Similar patterns of transposon overexpression are observed in *aub* and *ago3* mutants, which disrupt piRNA biogenesis (Li et al., 2009). Mutations in established piRNA pathway genes and in the *rhino* locus thus disrupt transposon silencing, independent of transposition mechanism.

piRNAs from the *suppressor of stellate* locus silence the *Stellate* gene during male germline development, and Stellate protein overexpression leads to Stellate crystal formation during spermatogenesis (Aravin et al., 2001; Bozzetti et al., 1995; Livak, 1984, 1990; Palumbo et al., 1994). However, *rhi* mutations do not lead to Stellate crystal formation or compromise male fertility (Figure S3 and data not shown).

HP1 and several genes in the piRNA pathway have been implicated in position effect variegation, which is linked to spreading of heterochromatin from centromeric and telomeric regions (Elgin and Grewal, 2003; Pal-Bhadra et al., 2004). However, neither *rhino* nor *armi* led to statistically significant changes in the expression of any protein coding genes, including the 613 annotated heterochromatic genes (Smith et al., 2007) (Figures 2D and 2E; green points indicate heterochromatic genes). piRNA pathway and *rhi* mutations thus do not produce changes in heterochromatin organization sufficient to alter protein coding gene expression during oogenesis.

Figure 2A shows a genome browser view of the region containing the heterochromatic gene *jing*. Expression of exons that comprise the mature *jing* transcript are essentially identical in w^{1118} and *rhi*, but expression of a *flea* transposon located in a major intron increases 7-fold (FDR < 0.02), and several transposons in the intergenic regions near *jing* are also overexpressed (Figure 2A, *rhino,* pink bars). The repeated nature of natural transposons and the design of the arrays makes it impossible to determine which specific transposon copy or copies are overexpressed, but we can conclude that at least one member of the

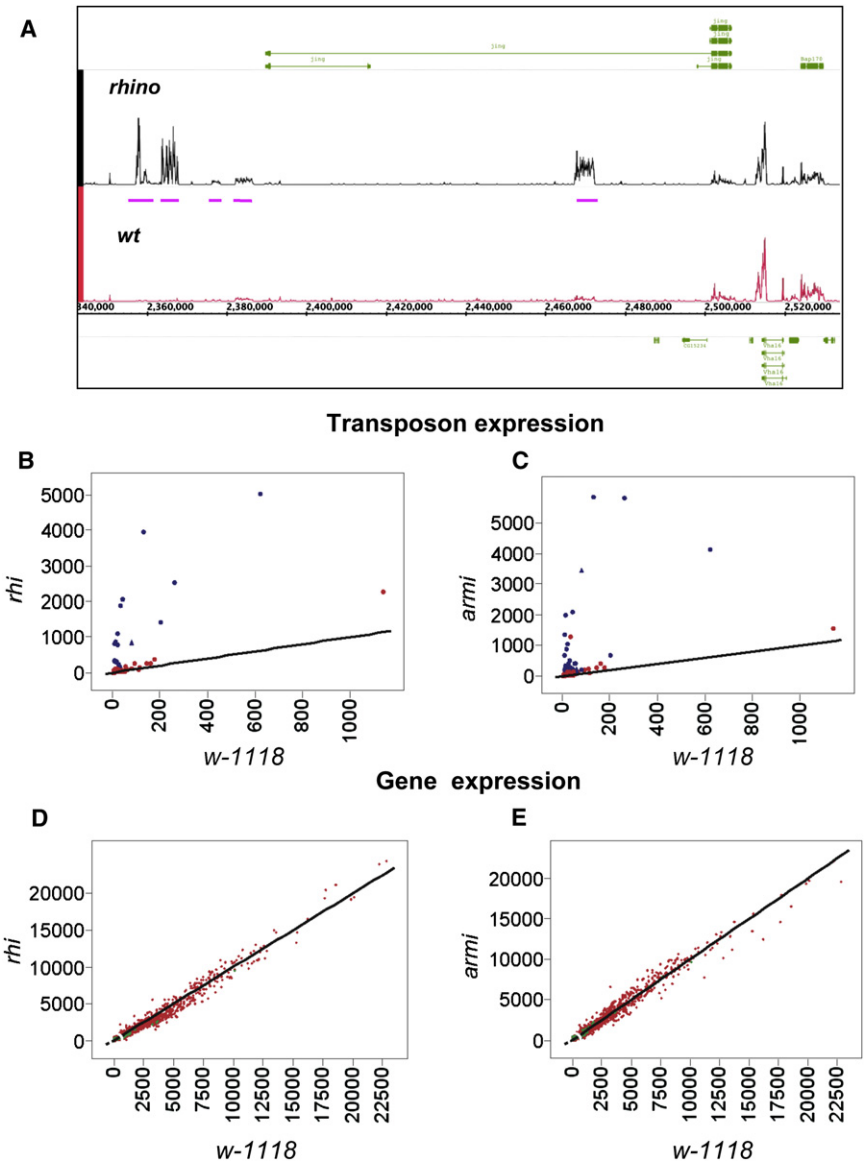

Figure 2. Gene and Transposon Expression in *rhi* Mutant Ovaries

(A) Genome browser view of tiling array data near *jing*, a protein-coding gene in pericentromeric heterochromatin on chromosome 2R. Expression of *jing* exons (green bars) is unaltered by *rhi* mutants. However, several intronic and extragenic transposons are significantly overexpressed (pink bars).

(B and C) Genome-wide analysis of transposon family expression in *rhi* and *armi* mutants. Tiling arrays were used to quantify expression of 95 transposon families in *rhi*, *armi*, and *w-1118* controls. Graphs show expression in *rhi* and *armi* plotted against expression in *w-1118*. The lines intercept the origin and have a slope of 1, and thus indicate equal expression in both genotypes. Significantly overexpressed transposon families are indicated by blue data points.

(D and E) Genome-wide comparison of protein coding gene expression in *rhi* and *armi* mutants, plotted against expression in *w1118*. Heterochromatic genes are indicated by green data points, and euchromatic genes are indicated by red data point. Both classes cluster around the diagonal, indicating similar expression levels in mutant and controls.

transposon family is overexpressed. Over 1300 protein coding genes carry transposon insertions within introns, and thus have primary transcripts that could base pair with piRNAs. This includes *ago3,* which encodes an Arognaute protein that is expressed in the female germline and is required for ping-pong amplification of piRNAs (Li et al., 2009). Our array studies show that expression of *ago3,* and the other protein coding genes carrying intronic transposon insertions, does not significantly change in *rhi* or *armi* mutants (Figures 2D and 2E and data not shown). These observations suggest that piRNA-dependent silencing may be imposed after splicing, which removed transposon homology from protein coding genes.

Rhi Localization

To define the subcellular distribution of Rhi, we generated a GFP-*rhi* transgene and raised anti-Rhi antibodies, which were used to localize the protein in vivo and immunolabel whole-mount egg chambers. Both methods revealed germline-specific nuclear foci that are present throughout oogenesis (Figures 3A–3D). In addition, germline-specific expression of the GFP-Rhi fusion protein rescued fertility and axial patterning in *rhi* mutations (Table S1). Rhi thus appears to function specifically within the germline cells of the ovary.

To determine whether Rhi foci are associated with centromeres, we labeled for Rhi and CID, the *Drosophila* homolog of the centromere-specific, histone H3-like CENP-A (Blower and Karpen, 2001). Rhi accumulated in regions adjacent to most CID foci in germline nuclei, consistent with localization to pericentromeric heterochromatin (Figures 3E–3G). However, many Rhi foci were not obviously linked to CID. Some of these foci could be linked to telomeres or other chromatin domains. Resolving this question will require higher-resolution molecular approaches.

To determine whether Rhi localization depends on the piRNA pathway, we immunolabeled egg chambers mutant for *aub* and *armi*. Rhino localization to nuclear foci was not disrupted by either mutation (Figures 3A–3C). In striking contrast, *rhi* mutations disrupt localization of Aub and Ago3 to nuage, a perinuclear structure implicated in RNA processing (Figures 3H, 3I, 3L, and 3M). Vasa is a core component of nuage, and perinuclear localization of Vasa was also lost in *rhi* mutants (Figure S4). Piwi localizes to nuclei in both germline cells and the somatic follicle cells. In wild-type ovaries, Piwi is most abundant in

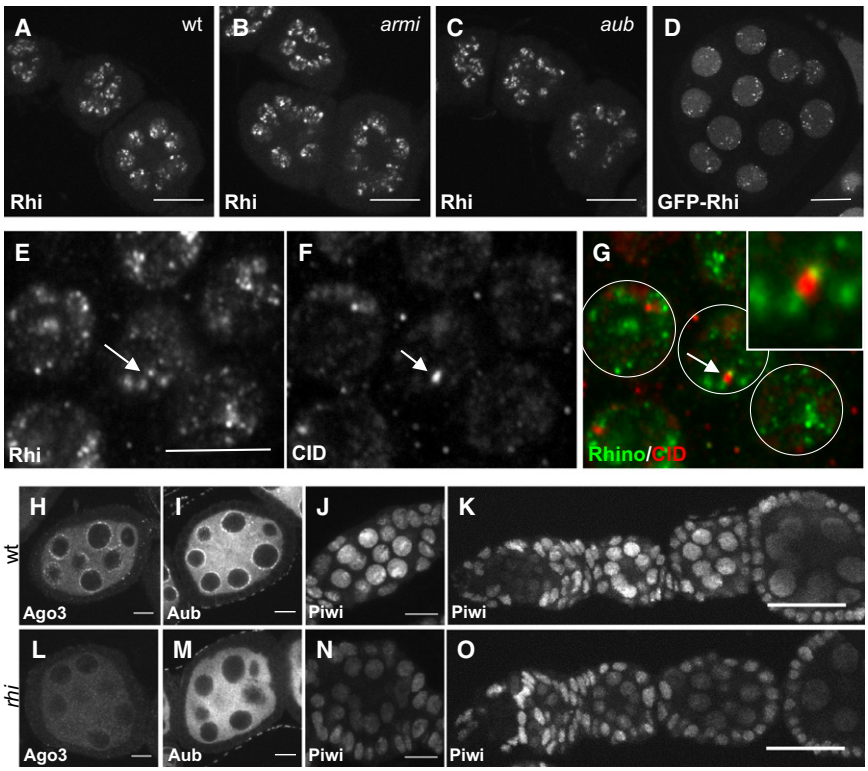

Figure 3. Rhi Localization Is Independent of the piRNA Pathway, but Localization of the PIWI Proteins Ago3 and Aub Requires Rhi

(A–C) Rhi localization appears similar in wild-type (A), *armi* (B), and *aub* (C) stage 2 to stage 4 egg chambers. Projections of five serial 1 μm optical sections are shown. Scale bars represent 20 μm.

(D) GFP-Rhi transgene shows localization pattern similar to endogenous Rhi detected with anti-Rhi antiserum in the germline nuclei of stage 4–5 egg chambers. The scale bar represents 10 μm.

(E–G) Wild-type ovaries immunostained with (E and G) anti-Rhi antiserum and (F and G) anti-CID antibody show that some Rhi foci localize adjacent to CID foci (arrows) consistent with binding to peri-centromeric heterochromatin in some but not all chromosomes. The scale bar represents 5 μm.

(H–O) *rhi* mutation disrupts localization of PIWI class Argonautes. Stage 4–5 (H, I, L, and M), stage 2–3 (J and N), and germarium to stage 3–4 egg chambers (K and O) of wild-type and *rhi* mutant ovaries were immunostained with corresponding antibodies. Projections of three serial 1 μm optical sections are shown. Scale bars represent 10 μm (H, I, J, L, M, and N) and 20 μm (J, K, and O). Wild-type localization of Ago3 and Aub proteins to perinuclear nuage is disrupted in *rhi* mutants. Piwi protein localizes to the nuclei of both germline and somatic cells in wild-type egg chambers. Only germline nuclear localization of Piwi in early stages is disrupted by mutations in *rhi*.

germline nuclei during early stages of oogenesis (Figure 3K). In *rhi* mutants, nuclear localization of Piwi is reduced during these early stages (Figures 3N and 3O). However, in later-stage egg chambers, which make up the bulk of the ovary, Piwi localization in *rhi* is similar to wild-type controls (Figures 3J, 3K, 3N, and 3O). These findings suggest *rhi* functions upstream of Ago3 and Aub, but may have a less critical role in Piwi-dependent processes.

piRNA Expression Is Ablated for Most Transposon Families in *rhino* Mutants

To determine whether Rhi is required for piRNA expression, we sequenced small RNAs from control and *rhi* mutant ovaries. Unlike miRNAs, piRNAs carry 2′ methoxy, 3′ hydroxy termini that render them resistant to oxidation and stabilize these RNAs in vivo (Vagin et al., 2006). To enrich for piRNAs and increase effective sequencing depth, we oxidized RNA samples prior to library construction and sequencing and normalized the data to surviving noncoding RNA fragments (Ghildiyal et al., 2008; Seitz et al., 2008) (see Table S3 for sequencing statistics). These studies indicate that *rhi* mutations reduce total piRNA abundance by approximately 80% (Figures 4A and 4B). Northern blotting for specific piRNAs and miRNAs support these findings (Figure S5). Defects in 3′ modification destabilize piRNAs and would lead to preferential loss of piRNAs in oxidized samples. We therefore deep sequenced unoxidized RNAs and normalized piRNA abundance to miRNAs. These studies confirm that *rhi* mutations reduce piRNA abundance by 80%, and indicate that this reduction does not result from a defect in end modification (data not shown).

The majority of *Drosophila* piRNAs are derived from transposons and other repeated elements (Aravin et al., 2003; Brennecke et al., 2007). We analyzed the impact of *rhi* mutations on piRNA expression from 95 families with at least 500 matching reads in control samples (Table S3) (Li et al., 2009). *rhi* mutations lead to a 50% or greater reduction in antisense piRNA abundance for 83% of these transposon families, and a 98% reduction in antisense piRNAs for approximately 30% of these elements (Figure S7). For 66 of 95 families, both sense and antisense piRNAs are reduced. For example, *rhi* mutations nearly eliminate sense and antisense piRNAs from the telomeric transposon *HeT-A* (Figure 5A). Eight transposon families continue to express at least 50% of wild-type sense strand piRNAs but show an 80% or greater reduction in antisense piRNAs. The *jockey* element falls into this class. Mutations in *rhi* reduce sense strand piRNAs linked to *jockey* by only 10%, but antisense strand piRNAs are reduced by 95% (Figure 4B, *jockey*). For all of the transposon families that show reduced antisense piRNAs, including those that retain sense strand piRNAs, there is a clear reduction in opposite strand piRNAs that overlap by 10 nt, consistent with defects in ping-pong amplification (Figures 5Ac and 5Bc). A comparison of the p values for the 10 nt overlap bias across all transposon families confirms that the loss of ping-pong pairs in *rhi* is very highly significant (Figure S6, p = 3e-10). The loss of species that overlap by 10nt is also clear from an analysis of total piRNAs (Figures 4C and 4D). The *rhi* mutations thus lead to a near collapse of the ping-pong cycle amplification cycle.

Only 10 of 95 transposon families continue to express antisense piRNAs at or above 75% of wild-type levels in *rhi* mutants

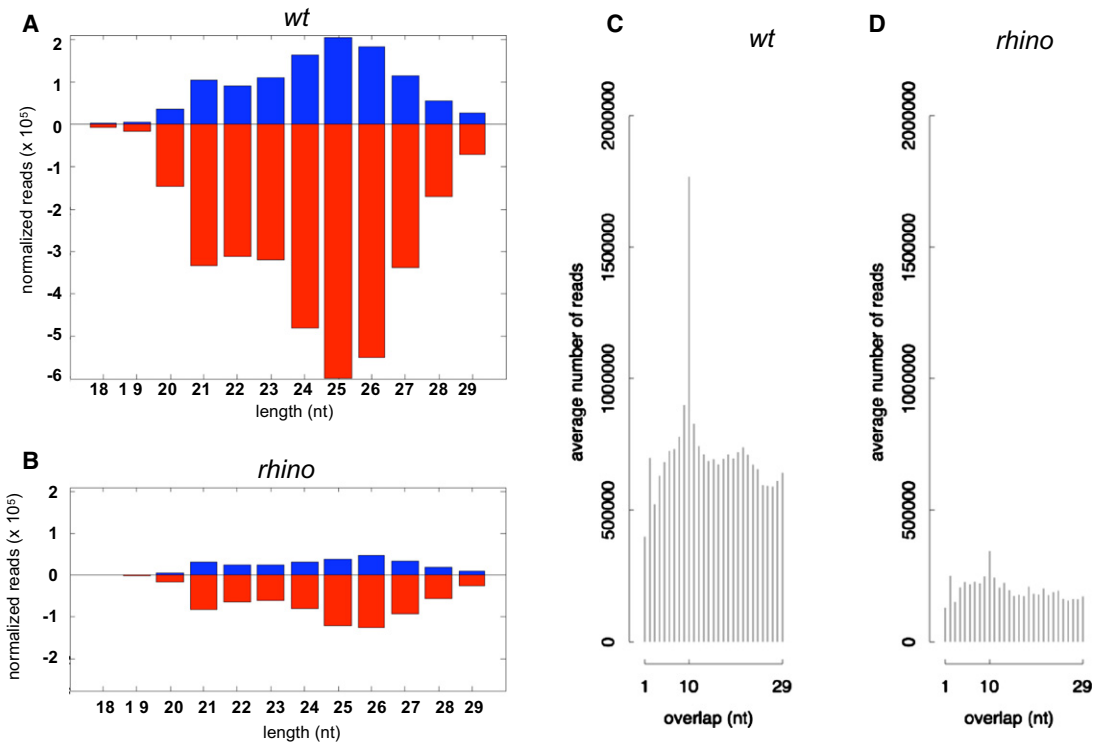

Figure 4. piRNA Production in *rhi* Mutants

(A) Length histogram of piRNAs expressed in wild-type ovaries.

(B) Length histogram of piRNAs produced in *rhi* mutants. Sense and antisense piRNAs are reduced by approximately 80%, and peak length shifts from 25 nt to 26 nt.

(C) Histogram of overlapping sense and antisense piRNA in wild-type ovaries, showing a pronounced peak at 10 nt, characteristic of ping-pong amplification.

(D) Histogram of overlapping sense and antisense piRNA in *rhi* mutant ovaries. The 10 nt peak is nearly eliminated, suggesting a breakdown in the ping-pong amplification cycle.

(*blood*, *mdg-1*, *Tabor*, *Stalker*, *Stalker 2*, *Stalker3*, *Stalker4*, *412*, *297*, *gypsy 5*; Table S4). Eight of these families (*blood*, *mdg-1*, *Tabor*, *Stalker*, *Stalker 2*, *Stalker3*, *Stalker4*, *412*) also show an increase in sense strand piRNAs (Figures 5Ca and S8). The sense strand piRNAs generally map to the same regions as peaks of antisense piRNAs (Figure 5Ca, *blood*; Figure S8). This pattern could indicate that antisense strand piRNA direct production of the sense strand piRNAs. Alternatively, specific regions within full-length elements or fragments of elements that lie within specific clusters may be preferentially utilized during piRNA production. The available data cannot distinguish between these alternatives.

An analysis of piRNAs encoded by the ten transposon families that show Rhi-independent piRNA production revealed three patterns with respect to overlapping sense and antisense species. The overlapping piRNAs encoded by *Stalker3* did not show a statistically significant ($p > 0.001$) 10 nt overlap bias in either wild-type or *rhi* mutants, indicating that their production is independent of ping-pong amplification. However, six families showed a statistically significant 10 nt overlap peak in both wild-type and *rhi* mutants, indicating that at least some of the piRNAs are produced by a ping-pong cycle that is independent of Rhi (*Tabor*, *Stalker*, *Stalker 2*, *Stalker4*, *412*, *297*; Figure S8). The final class of elements includes *blood*, *mdg1*, and *gypsy5*, which show a statistically significant ping-pong peak in wild-type, but loose the 10 nt overlap bias in *rhi* mutants (Figure 5Cc, *blood*; Figure S8). For this class, Rhi thus appears to promote production of only a subset of piRNAs through ping-pong amplification. Intriguingly, *rhi* leads to a 10-fold increase in *blood* expression, suggesting the minor ping-pong pool of piRNAs may be critical to transposon silencing (Figure S9).

Overlapping ping-pong pairs show transposon family-specific nucleotide biases at positions 1 and 10 that appear to reflect the specific PIWI proteins that participate in the amplification cycle (Brennecke et al., 2007; Gunawardane et al., 2007). For example, elements for which sense strand piRNAs are primarily bound by Ago3 and antisense strand piRNAs are primarily bound by Aub, show an A bias at position 10 of the sense strand and a U bias at position 1 of the antisense strand (Brennecke et al., 2007; Gunawardane et al., 2007). Families that retain a statistically significant ping-pong peak generally retain the pattern of nucleotide bias observed in the wild-type (Figure S8), suggesting that *rhi* reduces the efficiency of the ping-pong amplification but does not alter the specific PIWI proteins that participate in the cycle.

Antisense piRNAs can base pair with target RNAs and guide cleavage by PIWI proteins and are therefore presumed to be the effectors of transposon silencing. To determine whether loss of antisense piRNAs in *rhi* mutants correlates with loss of

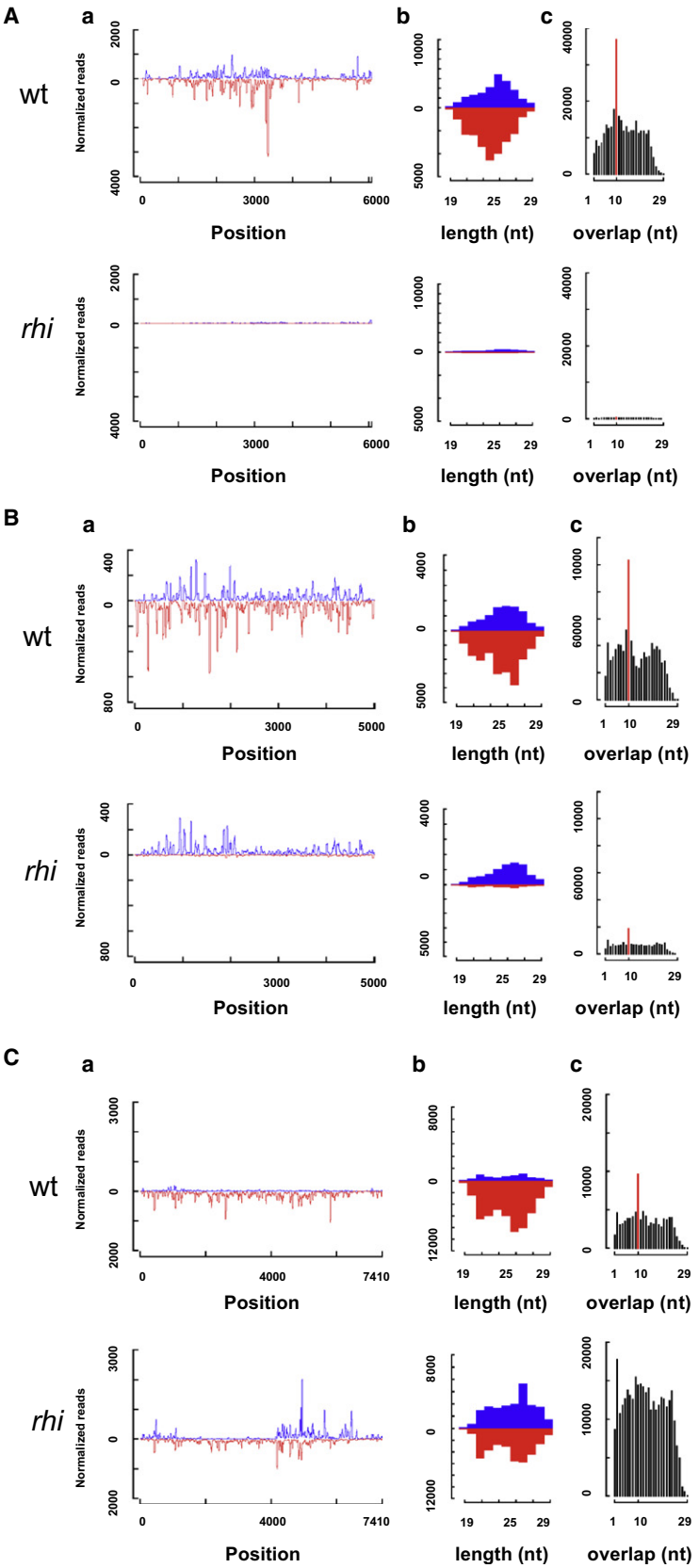

Figure 5. Transposon-Specific Changes in piRNA Abundance

(A) Sense and antisense piRNA reads mapping to the consensus *Het-A* sequence (Aa), length histograms for all *HetA* piRNAs (Ab), and frequency distribution of overlapping *HetA* piRNA (Ac).

(B) Sense and antisense piRNAs reads mapping to the consensus *jockey* sequence (Ba), length histograms for all *jockey* piRNAs (Bb), and frequency distribution of overlapping *jockey* piRNAs (Bc).

(C) Sense and antisense piRNA reads mapping to the consensus *blood* sequence (Ca), length histograms for all *blood* piRNAs (Cb), and frequency distribution of overlapping *blood* piRNA (Cc).

For the majority of transposons, including *HetA*, *rhi* mutations dramatically reduce sense and antisense piRNAs and nearly eliminate piRNA that overlap by 10 nt. For a subset of elements, represented by *jockey*, *rhi* leads to a loss of antisense piRNAs but no significant reduction in sense strand piRNAs. A very limited number of transposons, including *blood*, show no change or an increase in sense strand piRNAs in *rhi* mutants. Mutations in *rhi* reduce piRNAs with a 10 nt overlap, even for elements that show an increase in piRNAs from opposite strands (Cc, *blood*). In (Ac), (Bc) and (Cc), A statistically significant 10 nt bias is indicated by a red bar. This is characteristic of the ping-pong amplification cycle.

silencing, we plotted the fold change in transposon expression (*rhi*/wt) against the fold-change in antisense piRNAs (Figure S9). All of the transposon families that increased in expression by 20-fold or greater in *rhi* mutants also showed a 75% or greater reduction in antisense piRNA abundance. In addition, none of the families that retained antisense piRNA expression at 80% or higher levels were significantly overexpressed (FRD < 0.02; Figure S9). However, many transposon families that show a reduction in antisense piRNAs abundance of over 10-fold did not show a statistically significant increase in expression (Figure S9). These elements may be silenced by a piRNA independent mechanism. Alternatively, piRNAs linked to these elements could silence these elements, perhaps by inhibiting translation, without altering target transcript stability.

piRNA Clusters

The majority of piRNAs match transposons that are present in multiple copies in the genome and cannot be uniquely mapped. However, piRNAs encoded by polymorphic transposons, divergent transposon fragments, or other unique sequences can be mapped. Chromosome profiles of these "unique mappers" reveal dispersed piRNA peaks in the euchromatic chromosome arms and a limited number of prominent pericentromeric and subtelomeric clusters, which appear to be the source of the majority of piRNAs (Brennecke et al., 2007). *rhi* mutations essentially eliminate piRNAs mapping to pericentromeric heterochromatin on all of the autosomes (Figures S10 and 6). By contrast, piRNAs mapping to the pericentromeric region on the X are retained (Figures S10 and 6).

Most heterochromatic clusters produce piRNAs from both the plus and minus genomic strands (dual-strand clusters), but two major pericentromeric clusters on the X chromosome produce piRNA almost exclusively from one strand (uni-strand clusters) (Brennecke et al., 2007). We find that *rhi* reduces by 30- to 50-fold piRNAs from both strands of the top 11 dual-strand clusters (Figure S11, blue bars). For example, piRNA production from cluster 1/42AB, which is estimated to produce up to 30% of all piRNAs (Brennecke et al., 2007), is reduced by over 97% (Figures 6A–6C). In striking contrast, piRNAs encoded by the uni-strand clusters are only minimally impacted by *rhi* (Figure S11, red bars). As shown in Figures 6B and 6D, piRNAs from cluster 2 are derived almost exclusively from one strand, and production of these piRNAs is nearly unchanged in *rhi* mutants (Figures 6B and 6D). This does not appear to reflect expression of cluster 2 piRNAs exclusively in the somatic follicle cells, since Ago3 is germline specific and *ago3* mutations reduce piRNAs linked to this locus by close to 20-fold (Figure S12). In addition, unique piRNAs mapping to this cluster immunoprecipitate with the germline specific PIWI proteins Aub and Ago3 (Figure S12). Both dual-strand and uni-strand clusters thus appear to be expressed in the germline, but *rhi* mutations only disrupt piRNA production by the dual-strand clusters. Consistent with these findings, nine of the ten transposon families that continue to express high levels of antisense piRNAs in *rhi* (75% of wild-type or greater) have insertions in one or both of the major uni-strand clusters (Table S5).

To determine whether Rhino protein associates with clusters, we performed chromatin immunoprecipitation (ChIP) using anti-GFP antibodies and flies expressing a functional Rhino-GFP transgene specifically in the germline. To control for nonspecific binding, precipitation was performed using nonimmune IgG on chromatin from ovaries expressing the GFP-rhino transgene. Additionally, anti-GFP antibodies were used on chromatin isolated from wild-type flies that do not express the GFP fusion. Quantitiative PCR (qPCR) assays showed only background signal in both of these control reactions (data not shown). The anti-GFP fractions were assayed for three regions of cluster 1/42AB, two regions of cluster 2, two regions in the heterochromatic protein coding genes *jing* and *pld* that flank the 42A/B cluster, and the euchromatic protein coding genes *rp49* and *ry* (Figure 6G). GFP-Rhi binding, measured as a fraction of input chromatin, was enriched at all three sites in the dual-strand cluster relative to the euchromatic protein coding genes (Figure 6F). By contrast, the two sites in uni-strand cluster 2 showed no enrichment relative to *rp49* or *ry* controls (Figure 6F). Regions in the two heterochromatic genes immediately flanking the 42A/B cluster showed binding that was 3- to 4-fold lower than the peak region in the cluster (1A) and appoximately 3-fold higher than binding to euchromatic genes. Rhino thus appears to be enriched at dual-strand heterochromatic clusters and may spread somewhat beyond the computationally defined limits of these clusters.

Cluster Transcription

The piRNA clusters are proposed to produce long precursor RNAs that are processed to form primary piRNAs, which in turn trigger the ping-pong amplification cycle by targeting sense strand transposon transcripts. To determine whether Rhino is required for RNA production by clusters, we used quantitative reverse transcriptase (RT)-PCR to assay RNAs derived from both strands of cluster 1/42AB, cluster 2, and *flam*. Reactions without RT produced no significant signal, and the low level of signal obtained in the absence of the strand specific RT primers was subtracted from the signal obtained with the strand specific primers. Consistent with production of piRNAs from both genomic strands, we detected longer RNAs from both strands at two independent locations in cluster 1/42AB (Figure 6E, blue bars). Significantly, RNAs from both strands were nearly eliminated in *rhi* homozygous mutants (Figure 6E, red bars). At cluster 1 and *flam,* which produce piRNA almost exclusively form the plus strand (Figure 6D) (Brennecke et al., 2007), RT-PCR detected RNA from only the plus strands (Figure 6F, blue bars). In striking contrast to cluster 1/42AB, *rhi* mutations led to a slight increase in plus strand transcript from cluster 2 and only a modest decrease in plus strand RNA from *flam.* These observations suggest that Rhino promotes production of precursor RNAs from dual-strand cluster 1/42AB, and possibly all dual-strand clusters.

Brennecke et al. (2007) proposed that antisense piRNAs derived from the clusters initiate ping-pong amplification by cleaving sense strand transcripts from target transposons. However, unique piRNAs derived from opposite strands of cluster1/42AB show a strong 10 nt overlap bias (Figure S13), indicating that they are produced by ping-pong processing of precursor RNAs derived from the cluster. Antisense piRNAs derived through cluster based ping-pong amplification thus

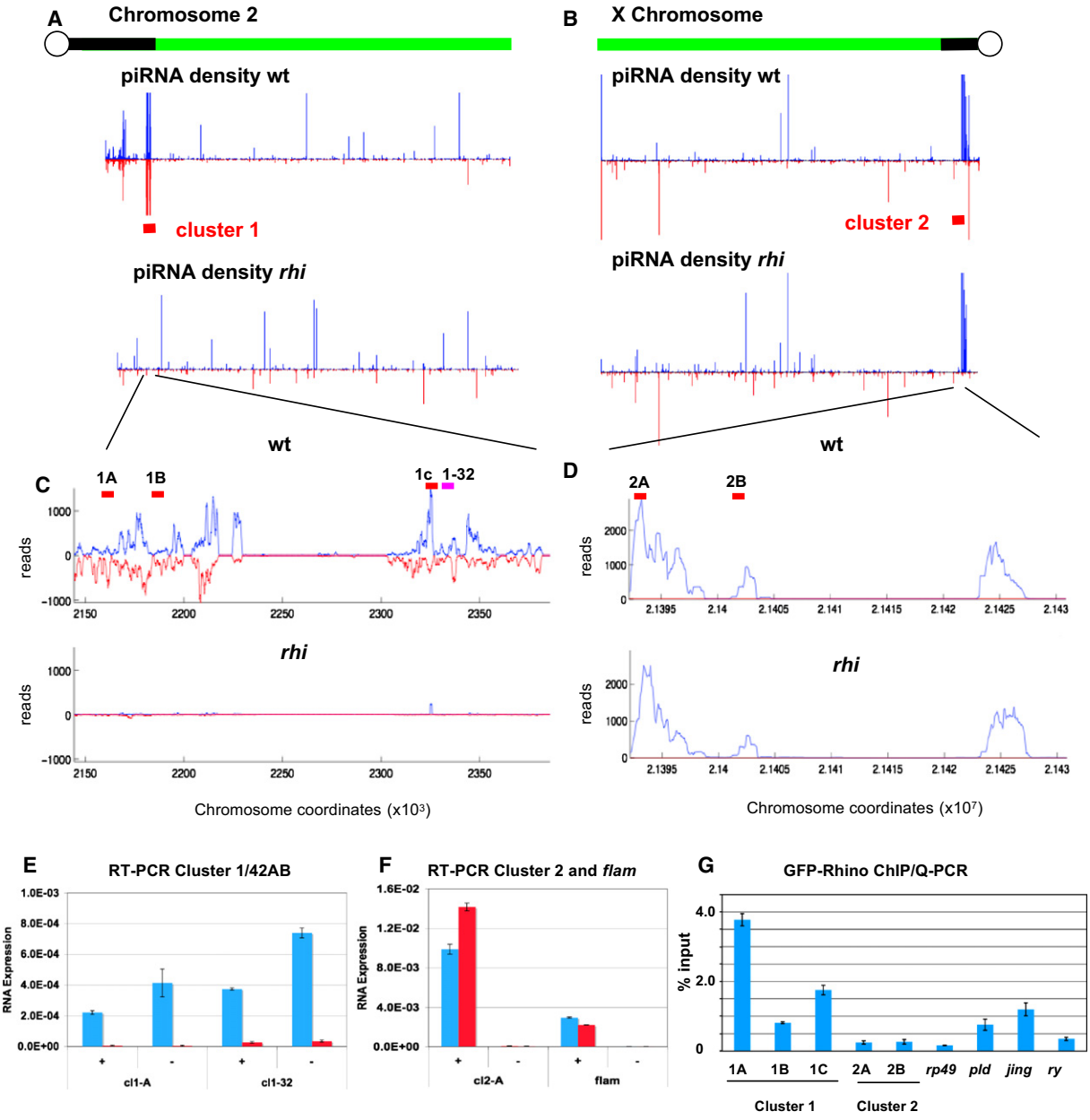

Figure 6. Rhino Is Required for piRNA Production by Dual-Strand Heterochromatic Clusters

(A and B) Chromosome 2R and X density profiles of uniquely mapping plus (blue) and minus (red) strand piRNAs in wild-type and *rhi* mutants. piRNAs map to dispersed loci on the chromosome arms and prominent heterochromatic clusters. Pericentromeric piRNAs from chromosome 2R (A), and all other autosomes (Figure S10) are dramatically reduced in *rhi* mutants. Pericentromeric piRNAs on the X chromosome show relatively little change.

(C and D) Higher-resolution maps of clusters 1 and 2, which map to the indicated regions on 2R and X, respectively. Mutations in *rhi* nearly eliminated piRNAs encoded by cluster 1, which is the major dual-strand cluster, but have little impact on piRNAs from cluster 2, which is the major uni-strand cluster.

(E and F) Quantitative strand-specific RT-PCR for RNA derived from dual-strand cluster 1 (E) and uni-strand clusters 2 and *flam* (F). In wild-type ovaries, RNA is detected from both the plus (+) and minus (–) strands of cluster 1, at two independent locations (F, cl1-A and cl1-32, blue bars). RNAs from both strands of cluster 1 are dramatically reduced in *rhi* mutants (red bars). Significant levels of RNA are only detected from the plus strand of cluster 2 and *flam* (F, blue bars), and *rhi* does not block expression of these RNAs (F, red bars).

(G) Chromatin immunoprecipitation/quantitative PCR analysis of Rhino binding to cluster 1/42AB, the euchromatic genes *rp49* and *ry*, and the heterochromatic genes *pld* and *jing*, which flank cluser 1. Rhino protein is highly enriched at cluster 1 relative to cluster 2 and the euchromatic genes. The protein-coding genes flanking cluster 1 show intermediate levels of binding, suggesting that Rhino may spread to regions flanking the dual-strand clusters. Anti-GFP antibodies were used to precipitate Rhino-GFP from crosslinked ovary chromatin fractions.

The approximate positions of the qPCR primer pairs used in ChIP and RT-PCR reactions are indicated by the red bars in (C) and (D). The pink bar in (C) indicates the approximate position of an additional primer pair used in RT-PCR.

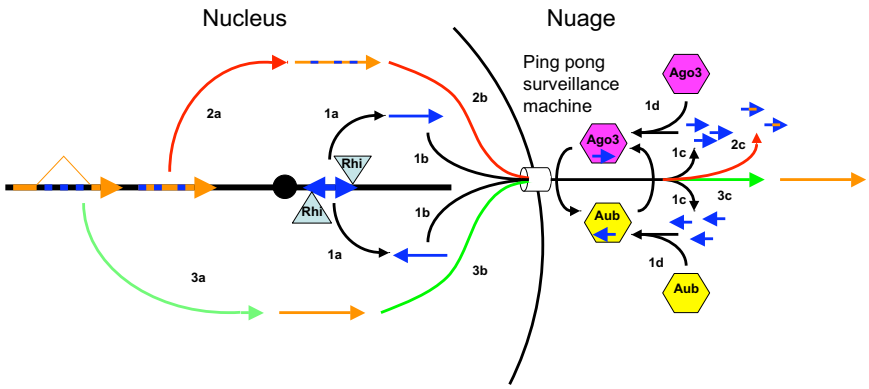

Figure 7. Model for Rhino-Dependent Transposon Silencing

Step 1 (black arrows): Rhino binds to dual-strand clusters and promotes production of RNAs from both genomic strands (1a), which are exported from the nucleus (1b) and processed into piRNAs by a ping-pong cycle driven by Ago3 (pink hexagon) and Aub (yellow hexagon), localized to the perinuclear nuage (1c).

Step 2 (red arrows): Transposons carrying piRNA homology are transcribed (2a), exported from the nucleus (2b), and degraded as they encounter the "ping-pong surveillance machine" within the nuage (2c).

Step 3 (green arrows): Protein-coding genes with intronic transposon insertions are spliced, which removes piRNA homology (3a). These transcripts are exported from the nucleus (3b) escape recognition by the surveillance system, and are translated (3c). Sequences matching piRNAs are indicated by blue. Other transcribed regions are in orange.

appear to target sense strand RNAs derived from functional transposons located throughout the genome.

DISCUSSION

piRNAs encoded by transposon-rich heterochromatic clusters have been proposed to initiate a ping-pong cycle that amplifies the piRNA pool and mediates transposon silencing (Brennecke et al., 2007; Lin, 2007; O'Donnell and Boeke, 2007). However, the mechanisms of piRNA biogenesis and silencing are not well understood, and it is unclear how the piRNA clusters are differentiated from other chromatin domains. We show that the HP1 homolog Rhino is required for production of piRNAs from dual-strand clusters and associates with the major 42AB cluster by ChIP. Significantly, we also identify putative piRNA precursor RNAs from both strands of the 42AB cluster and show that Rhino is required for production of these RNAs. These findings lead us to propose that Rhi binding promotes transcription of dual-strand clusters, and that the resulting RNAs are processed to form primary piRNAs that drive the ping-pong amplification cycle and transposon silencing (Figure 7, black pathway).

While Rhino protein appears to be restricted to germline nuclei, *rhi* mutations disrupt perinuclear localization of Ago3 and Aub (Figure 3), which catalyze the ping-pong amplification cycle (Li et al., 2009). Mutations in *krimper*, which encodes a component of the perinuclear nuage, also disrupt transposon silencing and piRNA production (Lim and Kai, 2007). piRNA silencing and nuage assembly thus appear to be codependent processes. These observations, with our finding that protein coding genes carrying piRNA homology within introns escape silencing by the piRNA pathway (Figure 2A), suggest that transcripts are scanned for piRNA homology within the nuage, after splicing and nuclear export. Mature protein coding mRNAs thus pass through the nuage and are translated because piRNA homology has been removed by splicing. By contrast, mature transposon transcripts carry piRNA complementarity are recognized by the perinuclear ping-pong machine, leading to destruction. Interestingly, mutations in the mouse *maelstrom* gene disrupt nuage and lead to male sterility and significant overexpression of LINE-1 elements (Soper et al., 2008). Nuage may therefore have a conserved function in transposon RNA surveillance and silencing.

In *S. pombe,* siRNAs bound to Ago1 appear to recruit HP1 to centromeres through interactions with nascent transcripts, thus triggering heterochromatin assembly and transcriptional silencing. Our data indicate that the HP1 homolog Rhino is required for transposon silencing, but this process appears to be mechanistically distinct from centromeric heterochromatin silencing in yeast. For example, localization of the Rhino HP1 homolog to nuclear foci is independent of piRNA production, and Rhino binding appears to promote transcription of heterochromatic clusters. This in turn generates piRNAs that may direct silencing through posttranscriptional target cleavage. However, piRNAs bound to PIWI proteins have been implicated in heterochromatin assembly in somatic cells, and this process could be related evolutionarily to heterochromatin assembly in fission yeast.

Intriguingly, *rhi* is a rapidly evolving gene, and all three Rhi protein domains (chromo, chromo shadow, and hinge) show evidence of strong positive selection (Vermaak et al., 2005). On the basis of these observations, Vermaak et al. (2005) proposed that *rhino* is involved in a genetic conflict within the germline. The observations reported here suggest that the conflict between transposon propagation and maintenance of germline DNA integrity drives *rhi* evolution, and that the heterochromatic dual-strand clusters have a key role in this battle. Rhino appears to define heterochromatic domains that produce transposon silencing piRNAs. Rhino could therefore have evolved to bind transposon integration proteins, which would promote transposition into clusters and production of *trans*-silencing piRNAs. In this model, the transposon integration machinery would evolve to escape Rhino binding and silencing. The rapid pace of *rhino* evolution makes identification of homologs in other species difficult (Vermaak et al., 2005), but the conserved role for piRNAs in germline development suggests that HP1 variants may have critical roles in the conflict between selfish elements and genome integrity in other species, including humans.

EXPERIMENTAL PROCEDURES

Drosophila Stocks

All animals were raised at 25°C. *Oregon R*, w^{1118} and cn^1; ry^{506} were used as controls, as noted. The following alleles were used: mnk^{P6} (Brodsky et al., 2004; Takada et al., 2003); $rhi^{KG00910}$ (rhi^{KG}) and rhi^{02086} (rhi^2) (Volpe et al., 2001); $armi^{72.1}$ and $armi^1$ (Cook et al., 2004); $mei41^{D3}$, (Hari et al., 1995; Hawley and Tartof, 1983); and P[*lacW*]*mei-W68*^{K05603}, *mei-W68*^{1} (McKim and Hayashi-Hagihara, 1998). The mnk^{P6} allele was kindly provided by M. Brodsky (Brodsky et al., 2004). All other stocks were obtained from the Bloomington Stock Center, Bloomington, Indiana (http://flystocks.bio.indiana.edu/). Standard genetic procedures were used to generate double mutant combinations.

Immunohistochemistry

Antibody production is described in the Supplemental Experimental Procedures. Egg chamber fixation and whole-mount antibody labeling were performed as previously described (Theurkauf, 1994). Vas protein was labeled with rabbit polyclonal anti-Vas antibody (Liang et al., 1994) at 1:1000. Gurken protein was labeled with mouse monoclonal anti-Gurken antibody (obtained from the Developmental Studies Hybridoma Bank, University of Iowa) at 1:10. Rhi protein was labeled with a guinea pig polyclonal anti-Rhi antiserum developed by our group (see above) at 1:2000. Piwi, Aub, and Ago3 were labeled with rabbit polyclonal anti-Piwi, anti-Aub and anti-Ago3 antibodies developed for this study (see above) at 1:1000. Antibody against γ-H2Av was kindly provided by K. McKim (Gong et al., 2005) and egg chambers were labeled as described previously (Belmont et al., 1989). CID was labeled with an affinity-purified chicken anti-CID antibody provided by G. Karpen at 1:100 (Blower and Karpen, 2001). HOAP was labeled with a polyclonal rabbit anti-Hoap antibody generated by our group (see above) at 1:1000. Rhodamine-conjugated phalloidin (Molecular Probes) was used at 1:100 to stain F-Actin, and TOTO3 (Molecular Probes) was used at 1:500 (0.2 mM final concentration) to visualize DNA.

Labeled tissue was mounted and analyzed with a Leica TCS-SP inverted laser-scanning microscope as described previously (Cha et al., 2001).

GFP-Rhino Transgene

The GFP-Rhi transgene was generated by recombining the Rhi-DONR (see above) construct with a modified pCasper vector containing the GFP sequence and Gateway cloning cassette B (Invitrogen). The resulting vector contained GFP fused in frame to the N terminus of Rhino under the control of the Gal4 promoter. Transgenic animals were generated using standard embryo microinjection techniques at Genetic Services.

RNA Isolation and Tiling Array Hybridization

Total RNA from was isolated from manually dissected ovaries from 2- to 4-day-old flies with RNeasy (QIAGEN) according to the manufacturer's instructions. The RNA was quantified by absorbance at 260 nm. Three independent RNA isolates from each genotype was then assayed as follows: Double-stranded cDNA was prepared with the GeneChip WT Amplified Double-Stranded cDNA Synthesis Kit (Affymetrix). DNA was labeled with the GeneChip WT Double-Stranded DNA Terminal Labeling Kit (Affymetrix). Labeled DNA was hybridized to GeneChip *Drosophila* Tiling 2.0R Arrays (Affymetrix) with the GeneChip Hybridization, Wash, and Stain Kit (Affymetrix) at the University of Massachusetts Medical School genomic core facility.

To determine whether genetic background or DNA damage significantly alters gene or transposon expression, we assayed ovarian RNA isolated from two common laboratory strains (*w-1118* and *cn,bw*), the meiotic repair mutant *okra,* the DNA damage signaling mutant *mnk*, and *mnk;okra* double mutants. Pairwise comparisons show little difference in genome wide patterns of gene or transposon expression in any of these five strains (Figure S12). The background for the *rhi* heteroallelic combination used here is *cn*/+; *ry*/+, which is genetically wild-type. Since the *armi* allelic combination used here is in a homozygous *w-1118* background, this genotype was used a control in our array studies.

The tiling array data discussed in this publication have been deposited in NCBI's Gene Expression Omnibus (Edgar et al., 2002) and are accessible through GEO Series accession number GSE14370 (http://www.ncbi.nlm.nih.gov/geo/query/acc.cgi?acc=GSE14370).

Small RNA isolation, oxidation, and sequencing were performed as described elsewhere (Li et al., 2009). Bioinformatics methods, chromatin immunoprecipitation and strand specific RT-PCR procedures are described in the Supplemental Experimental Procedures.

SUPPLEMENTAL DATA

Supplemental Data include Supplemental Experimental Procedures, 14 figures, and six tables and can be found with this article online at http://www.cell.com/supplemental/S0092-8674(09)00853-8.

ACKNOWLEDGMENTS

We thank Celeste Berg for *rhi* mutant stocks, Maria Zapp and Ellie Kittler in the UMass Deep Sequencing Core and Phyllis Spartick in the UMass Genomics core for expert assistance with small RNA sequencing and tiling array analyses, and members of the Zamore, Weng, and Theurkauf labs for critical discussions during the course of these studies. The Genomics Core was supported by the Diabetes and Endocrinology research Center grant DK032502. This work was supported in part by grants from the National Institutes of Health to W.E.T. (HD049116) and P.D.Z. (GM62862 and GM65236). H.X. was supported in part by Pfizer.

Received: February 20, 2009
Revised: May 7, 2009
Accepted: July 2, 2009
Published online: September 3, 2009

REFERENCES

Aravin, A.A., Naumova, N.M., Tulin, A.V., Vagin, V.V., Rozovsky, Y.M., and Gvozdev, V.A. (2001). Double-stranded RNA-mediated silencing of genomic tandem repeats and transposable elements in the D. melanogaster germline. Curr. Biol. *11*, 1017–1027.

Aravin, A.A., Lagos-Quintana, M., Yalcin, A., Zavolan, M., Marks, D., Snyder, B., Gaasterland, T., Meyer, J., and Tuschl, T. (2003). The small RNA profile during Drosophila melanogaster development. Dev. Cell *5*, 337–350.

Belmont, A.S., Braunfeld, M.B., Sedat, J.W., and Agard, D.A. (1989). Large-scale chromatin structural domains within mitotic and interphase chromosomes in vivo and in vitro. Chromosoma *98*, 129–143.

Blower, M.D., and Karpen, G.H. (2001). The role of Drosophila CID in kinetochore formation, cell-cycle progression and heterochromatin interactions. Nat. Cell Biol. *3*, 730–739.

Bozzetti, M.P., Massari, S., Finelli, P., Meggio, F., Pinna, L.A., Boldyreff, B., Issinger, O.G., Palumbo, G., Ciriaco, C., Bonaccorsi, S., et al. (1995). The Ste locus, a component of the parasitic cry-Ste system of Drosophila melanogaster, encodes a protein that forms crystals in primary spermatocytes and mimics properties of the beta subunit of casein kinase 2. Proc. Natl. Acad. Sci. USA *92*, 6067–6071.

Brennecke, J., Aravin, A.A., Stark, A., Dus, M., Kellis, M., Sachidanandam, R., and Hannon, G.J. (2007). Discrete small RNA-generating loci as master regulators of transposon activity in Drosophila. Cell *128*, 1089–1103.

Brennecke, J., Malone, C., Aravin, A., Sachidanandam, R., Stark, A., and Hannon, G. (2008). An epigenetic role for maternally inherited piRNAs in transposon silencing. Science *322*, 1387–1392.

Brodsky, M.H., Weinert, B.T., Tsang, G., Rong, Y.S., McGinnis, N.M., Golic, K.G., Rio, D.C., and Rubin, G.M. (2004). Drosophila melanogaster MNK/Chk2 and p53 regulate multiple DNA repair and apoptotic pathways following DNA damage. Mol. Cell. Biol. *24*, 1219–1231.

Brower-Toland, B., Findley, S.D., Jiang, L., Liu, L., Yin, H., Dus, M., Zhou, P., Elgin, S.C., and Lin, H. (2007). Drosophila PIWI associates with chromatin and interacts directly with HP1a. Genes Dev. *21*, 2300–2311.

Buhler, M., Verdel, A., and Moazed, D. (2006). Tethering RITS to a nascent transcript initiates RNAi- and heterochromatin-dependent gene silencing. Cell *125*, 873–886.

Carmell, M.A., Girard, A., van de Kant, H.J., Bourc'his, D., Bestor, T.H., de Rooij, D.G., and Hannon, G.J. (2007). MIWI2 is essential for spermatogenesis and repression of transposons in the mouse male germline. Dev. Cell *12*, 503–514.

Cha, B.-J., Koppetsch, B., and Theurkauf, W.E. (2001). *In vivo* analysis of *bicoid* mRNA localization reveals a novel microtubule-dependent anterior axis specification pathway. Cell *106*, 35–46.

Chambeyron, S., Popkova, A., Payen-Groschene, G., Brun, C., Laouini, D., Pelisson, A., and Bucheton, A. (2008). piRNA-mediated nuclear accumulation of retrotransposon transcripts in the Drosophila female germline. Proc. Natl. Acad. Sci. USA *105*, 14964–14969.

Chen, Y., Pane, A., and Schupbach, T. (2007). Cutoff and aubergine mutations result in retrotransposon upregulation and checkpoint activation in Drosophila. Curr. Biol. *17*, 637–642.

Cook, H.A., Koppetsch, B.S., Wu, J., and Theurkauf, W.E. (2004). The Drosophila SDE3 homolog armitage is required for oskar mRNA silencing and embryonic axis specification. Cell *116*, 817–829.

Desset, S., Buchon, N., Meignin, C., Coiffet, M., and Vaury, C. (2008). In Drosophila melanogaster the COM locus directs the somatic silencing of two retrotransposons through both Piwi-dependent and -independent pathways. PLoS ONE *3*, e1526.

Edgar, R., Domrachev, M., and Lash, A.E. (2002). Gene Expression Omnibus: NCBI gene expression and hybridization array data repository. Nucleic Acids Res. *30*, 207–210.

Elgin, S.C., and Grewal, S.I. (2003). Heterochromatin: silence is golden. Curr. Biol. *13*, R895–R898.

Ghildiyal, M., and Zamore, P. (2009). Small silencing RNAs: an expanding universe. Nat. Rev. Genet. *10*, 94–108.

Ghildiyal, M., Seitz, H., Horwich, M.D., Li, C., Du, T., Lee, S., Xu, J., Kittler, E.L., Zapp, M.L., Weng, Z., and Zamore, P.D. (2008). Endogenous siRNAs derived from transposons and mRNAs in Drosophila somatic cells. Science *320*, 1077–1081.

Girton, J.R., and Johansen, K.M. (2008). Chromatin structure and the regulation of gene expression: the lessons of PEV in Drosophila. Adv. Genet. *61*, 1–43.

Gong, W.J., McKim, K.S., and Hawley, R.S. (2005). All paired up with no place to go: pairing, synapsis, and DSB formation in a balancer heterozygote. PLoS Genet. *1*, e67.

Gunawardane, L.S., Saito, K., Nishida, K.M., Miyoshi, K., Kawamura, Y., Nagami, T., Siomi, H., and Siomi, M.C. (2007). A slicer-mediated mechanism for repeat-associated siRNA 5′ end formation in Drosophila. Science *315*, 1587–1590.

Hari, K.L., Santerre, A., Sekelsky, J.J., McKim, K.S., Boyd, J.B., and Hawley, R.S. (1995). The mei-41 gene of D. melanogaster is a structural and functional homolog of the human ataxia telangiectasia gene. Cell *82*, 815–821.

Hawley, R.S., and Tartof, K.D. (1983). The effect of mei-41 on rDNA redundancy in Drosophila melanogaster. Genetics *104*, 63–80.

Houwing, S., Kamminga, L.M., Berezikov, E., Cronembold, D., Girard, A., van den Elst, H., Filippov, D.V., Blaser, H., Raz, E., Moens, C.B., et al. (2007). A role for Piwi and piRNAs in germ cell maintenance and transposon silencing in Zebrafish. Cell *129*, 69–82.

Jang, J.K., Sherizen, D.E., Bhagat, R., Manheim, E.A., and McKim, K.S. (2003). Relationship of DNA double-strand breaks to synapsis in Drosophila. J. Cell Sci. *116*, 3069–3077.

Klattenhoff, C., Bratu, D.P., McGinnis-Schultz, N., Koppetsch, B.S., Cook, H.A., and Theurkauf, W.E. (2007). Drosophila rasiRNA pathway mutations disrupt embryonic axis specification through activation of an ATR/Chk2 DNA damage response. Dev. Cell *12*, 45–55.

Li, C., Vagin, V.V., Lee, S., Xu, J., Ma, S., Xi, H., Seitz, H., Horwich, M.D., Syrzycka, M., Honda, B.M., et al. (2009). Collapse of germline piRNAs in the absence of Argonaute3 reveals somatic piRNAs in flies. Cell *137*, 509–521.

Liang, L., Diehl-Jones, W., and Lasko, P. (1994). Localization of vasa protein to the Drosophila pole plasm is independent of its RNA-binding and helicase activities. Development *120*, 1201–1211.

Lim, A.K., and Kai, T. (2007). Unique germ-line organelle, nuage, functions to repress selfish genetic elements in Drosophila melanogaster. Proc. Natl. Acad. Sci. USA *104*, 6714–6719.

Lin, H. (2007). piRNAs in the germ line. Science *316*, 397.

Livak, K.J. (1984). Organization and mapping of a sequence on the Drosophila melanogaster X and Y chromosomes that is transcribed during spermatogenesis. Genetics *107*, 611–634.

Livak, K.J. (1990). Detailed structure of the Drosophila melanogaster stellate genes and their transcripts. Genetics *124*, 303–316.

McKim, K.S., and Hayashi-Hagihara, A. (1998). mei-W68 in Drosophila melanogaster encodes a Spo11 homolog: evidence that the mechanism for initiating meiotic recombination is conserved. Genes Dev. *12*, 2932–2942.

Mevel-Ninio, M., Pelisson, A., Kinder, J., Campos, A.R., and Bucheton, A. (2007). The flamenco locus controls the gypsy and ZAM retroviruses and is required for Drosophila oogenesis. Genetics *175*, 1615–1624.

Modesti, M., and Kanaar, R. (2001). DNA repair: spot(light)s on chromatin. Curr. Biol. *11*, R229–R232.

O'Donnell, K.A., and Boeke, J.D. (2007). Mighty Piwis defend the germline against genome intruders. Cell *129*, 37–44.

Pal-Bhadra, M., Bhadra, U., and Birchler, J.A. (2002). RNAi related mechanisms affect both transcriptional and posttranscriptional transgene silencing in Drosophila. Mol. Cell *9*, 315–327.

Pal-Bhadra, M., Leibovitch, B.A., Gandhi, S.G., Rao, M., Bhadra, U., Birchler, J.A., and Elgin, S.C. (2004). Heterochromatic silencing and HP1 localization in Drosophila are dependent on the RNAi machinery. Science *303*, 669–672.

Palumbo, G., Bonaccorsi, S., Robbins, L.G., and Pimpinelli, S. (1994). Genetic analysis of Stellate elements of Drosophila melanogaster. Genetics *138*, 1181–1197.

Pane, A., Wehr, K., and Schupbach, T. (2007). zucchini and squash encode two putative nucleases required for rasiRNA production in the Drosophila germline. Dev. Cell *12*, 851–862.

Pelisson, A., Song, S.U., Prud'homme, N., Smith, P.A., Bucheton, A., and Corces, V.G. (1994). Gypsy transposition correlates with the production of a retroviral envelope-like protein under the tissue-specific control of the Drosophila flamenco gene. EMBO J. *13*, 4401–4411.

Pelisson, A., Payen-Groschene, G., Terzian, C., and Bucheton, A. (2007). Restrictive flamenco alleles are maintained in Drosophila melanogaster population cages, despite the absence of their endogenous gypsy retroviral targets. Mol. Biol. Evol. *24*, 498–504.

Prud'homme, N., Gans, M., Masson, M., Terzian, C., and Bucheton, A. (1995). Flamenco, a gene controlling the gypsy retrovirus of Drosophila melanogaster. Genetics *139*, 697–711.

Redon, C., Pilch, D., Rogakou, E., Sedelnikova, O., Newrock, K., and Bonner, W. (2002). Histone H2A variants H2AX and H2AZ. Curr. Opin. Genet. Dev. *12*, 162–169.

Saito, K., Nishida, K.M., Mori, T., Kawamura, Y., Miyoshi, K., Nagami, T., Siomi, H., and Siomi, M.C. (2006). Specific association of Piwi with rasiRNAs derived from retrotransposon and heterochromatic regions in the Drosophila genome. Genes Dev. *20*, 2214–2222.

Sarkaria, J.N., Busby, E.C., Tibbetts, R.S., Roos, P., Taya, Y., Karnitz, L.M., and Abraham, R.T. (1999). Inhibition of ATM and ATR kinase activities by the radiosensitizing agent, caffeine. Cancer Res. *59*, 4375–4382.

Sarot, E., Payen-Groschene, G., Bucheton, A., and Pelisson, A. (2004). Evidence for a piwi-dependent RNA silencing of the gypsy endogenous retrovirus by the Drosophila melanogaster flamenco gene. Genetics *166*, 1313–1321.

Seitz, H., Ghildiyal, M., and Zamore, P.D. (2008). Argonaute loading improves the 5′ precision of both MicroRNAs and their miRNA strands in flies. Curr. Biol. *18*, 147–151.

Smith, C.D., Shu, S., Mungall, C.J., and Karpen, G.H. (2007). The Release 5.1 annotation of Drosophila melanogaster heterochromatin. Science *316*, 1586–1591.

Soper, S.F., van der Heijden, G.W., Hardiman, T.C., Goodheart, M., Martin, S.L., de Boer, P., and Bortvin, A. (2008). Mouse maelstrom, a component of nuage, is essential for spermatogenesis and transposon repression in meiosis. Dev. Cell *15*, 285–297.

Takada, S., Kelkar, A., and Theurkauf, W.E. (2003). Drosophila checkpoint kinase 2 couples centrosome function and spindle assembly to genomic integrity. Cell *113*, 87–99.

Theurkauf, W.E. (1994). Immunofluorescence analysis of the cytoskeleton during oogenesis and early embryogenesis. Methods Cell Biol. *44*, 489–505.

Vagin, V.V., Sigova, A., Li, C., Seitz, H., Gvozdev, V., and Zamore, P.D. (2006). A distinct small RNA pathway silences selfish genetic elements in the germline. Science *313*, 320–324.

Verdel, A., and Moazed, D. (2005). RNAi-directed assembly of heterochromatin in fission yeast. FEBS Lett. *579*, 5872–5878.

Vermaak, D., Henikoff, S., and Malik, H.S. (2005). Positive selection drives the evolution of rhino, a member of the heterochromatin protein 1 family in Drosophila. PLoS Genet. *1*, 96–108.

Volpe, A.M., Horowitz, H., Grafer, C.M., Jackson, S.M., and Berg, C.A. (2001). Drosophila rhino encodes a female-specific chromo-domain protein that affects chromosome structure and egg polarity. Genetics *159*, 1117–1134.

Wang, X.Q., Redpath, J.L., Fan, S.T., and Stanbridge, E.J. (2006). ATR dependent activation of Chk2. J. Cell. Physiol. *208*, 613–619.